 doi:10.20944/preprints201805.0269.v1

Melt Processing and Characterization of Biodegradable Poly(butylene succinate-co-adipate)/hexadecylamine-Modified Layered Zinc Phenylphosphonate Nanocomposites

*Dong-Lin Kuo, Erh-Chiang Chen and Tzong-Ming Wu**

Department of Materials Science and Engineering, National Chung Hsing University, 250 Kuo Kuang Road, Taichung, Taiwan 402

***Corresponding author.** Tel.: +886 4 2287 2482; fax: +886 4 2285 7017. E-mail: tmwu@dragon.nchu.edu.tw (T. M. Wu)

 doi:10.20944/preprints201805.0269.v1

Abstract

Biocompatible and biodegradable poly(butylene succinate-co-adipate) (PBSA)/hexadecylamine-modified PPZn (m-PPZn) nanocomposites were prepared using a melt mixing process. Experimental results of wide-angle X-ray diffraction and transmission electron microscopy revealed that the stacking layers of the m-PPZn were partially intercalated and partially exfoliated into the PBSA polymer matrix. The isothermal crystallization kinetics of PBSA/m-PPZn nanocomposites were studied at the temperature range of 62−70 °C and the half-time for crystallization of 3 wt % PBSA/m-PPZn nanocomposite was reduced by 27−35% compared with that of pure PBSA. This finding suggests that the incorporation of m-PPZn might cause the heterogeneous nucleation and the subsequent crystallization growth, which enhances the isothermal crystallization rate of PBSA/m-PPZn nanocomposite. The biodegradation rates of PBSA using Lipase from *Pseudomonas sp.* increase as the contents of m-PPZn increase. The degradation behavior of the neat PBSA investigated using the change of weight-average molecular weight belongs to exo-type hydrolysis activity. It is necessary to point out that the change of degree of crystallinity and degradation rate are almost linearly proportional to the loading of hexadecylamine-modified PPZn. This finding would provide an important information for the manufacturing biodegradable PBSA nanocomposites.

Keywords: Poly(butylene succinate-co-adipate); Zinc phenylphosphonate; Nanocomposites; Crystallization; Biodegradation.

 doi:10.20944/preprints201805.0269.v1

INTRODUCTION

Biocompatible and biodegradable polymers have been attracted numerous attention owing to their promising biodegradability for environmental advantages [1]. Poly[(butylene succinate)-co-adipate] (PBSA), a semi-crystalline copolyester, shows plentifully desirable natures, including excellent chemical resistance, melt processibility, and thermal properties [2-4]. As a consequence of more flexible polymer chains and slower crystallization rate of PBSA, useful application has been limited [5]. To enhance these physical properties, the loading of rigid inorganic material served as the nucleation agent into the biodegradable PBSA could improve its properties [6-8].

Layered zinc phenylphosphonate (PPZn), a group of two-dimensional layered material, has received lots interest because of speed up the crystallization of various polymers [9-11]. However, the interlayer distance of PPZn is extremely small for the insertion of polymer chains into its interlayer gallery. To overcome this problem, organo-modifiers served as delamination compound to enlarge the interlayer spacing of PPZn have been applied [12, 13]. The biocompatible and nontoxic organo-modifiers was selected owing to the preparation of fully green nanocomposites. In the present study, the biocompatible and nontoxic hexadecylamine, a long-chain alkylamine, was used to manufacture the organically-modified PPZn (hereafter designated as m-PPZn) by co-precipitation technique.

Thus, the new biodegradable PBSA/hexadecylamine-modified PPZn nanocomposites used for completely green materials were prepared by a melt mixing process. The crystallization behavior and

Preprints (www.preprints.org) | NOT PEER-REVIEWED | Posted: 21 May 2018 doi:10.20944/preprints201805.0269.v1

biodegradation of PBSA/m-PPZn nanocomposites were studied systematically.

EXPERIMENTAL

Materials

Biodegradable PBSA (Bionolle 3001) was obtained provided by Showa Denko Co., Ltd. Hexadecylamine, polyoxyethylene bis(amine), phenylphosphonic acid, zinc nitrate, and Lipase from *Pseudomonas sp.* were provided from Sigma-Aldrich.

Experimental

Melt processing of PBSA/m-PPZn nanocomposites. Hexadecylamine-intercalated PPZns were prepared by a similar approach reported previously [12, 13]. The 1, 3 and 5 wt % PBSA/m-PPZn nanocomposites were fabricated by mixing the m-PPZn, PBSA, and polyoxyethylene bis(amine) at 105 °C using a single-screw extruder (Brabender Mix 30/50E) for 5 min. For comparison, the pure PBSA was produced using the same method. Consequently, the fabricated PBSA and PBSA/m-PPZn samples were hot pressed at 105 °C to make a film for subsequent analyses.

Enzymatic degradation of PBSA/m-PPZn nanocomposites. All specimens were placed in 24-well plates containing 1 ml/mg enzymatic solution for the biodegradation test. The enzymatic solution were prepared using 0.1 M phosphate buffer, pH = 7.4, at 37 °C with lipase from *Pseudomonas sp.*. The specimens were taken out at 1, 2, 3, and 4 days, washed with distilled water and vacuum dried. The degree of degradation was calculated using the equation: $Wweight_{loss}$ (%) = $100[(W_0 - W_t)/W_0]$, where W_0 corresponds to the original weight of a specimen and W_t represents the weight of a specimen after

Preprints (www.preprints.org) | NOT PEER-REVIEWED | Posted: 21 May 2018 doi:10.20944/preprints201805.0269.v1

different degradation times. The experimental data revealed here are the mean values of at least three measurements.

Nanocomposites Characterization and Testing

Structural Characterization. X-ray diffractometer (Bruker D8) equipped with a Ni-filtered Cu Kα radiation was used for the experiments of small-angle X-ray scattering (SAXS) and wide-angle X-ray diffraction (WAXD). The diffraction patterns of WAXD measurements were performed in the range of $2\theta = 1.5°–30°$ at a scanning rate of 1°/min. The degree of crystallinity was calculated by WAXD data. The q, defined as $q = (4\pi\sin\theta)/\lambda$, is the scattering vector in SAXS measurement. The Transmission electron microscopy (TEM) was carried out by a Hitachi HF-2000. The specimens of TEM experiments encapsulated in epoxy matrix were obtained by a Reichert Ultracut ultramicrotome. Field-emission scanning electron microscopy (JEOL JSM-6700F) was used to examine the surface morphologies of all samples. The surfaces of all samples were covered with gold to prevent charging.

Crystallization Behavior and Biodegradation Test. The isothermal crystallization behavior was carried out by a PerkinElmer Pyris Diamond DSC and all experiments were performed under a nitrogen atmosphere. All specimens were heated to 150 °C at a rate of 10 °C/min and held for 5 min to remove the residual crystals. Then, they were quickly quenched to proposed crystallization temperatures (T_{cs}) between 62 and 70 °C, and held to finish total crystallization. The growth of spherulite was obtained using a Zeiss optical microscope equipped with a Mettler FP-82 hot stage and crossed polarizers. All samples were heated to melt at 150 °C at a rate of 10 °C/min for 3 min to

Preprints (www.preprints.org) | NOT PEER-REVIEWED | Posted: 21 May 2018 doi:10.20944/preprints201805.0269.v1

remove previous thermal history. Consequently, the samples were then cooled rapidly to the T_{cs}. Optical microscopy was recorded at the proposed T_c for various times. For the degradation tests, the molecular weights of all samples were evaluated using gel permeation chromatography (GPC, Waters 717 Plus autosampler). Calibration was performed using polystyrene standards.

RESULTS AND DISCUSSION

Structural Characterization

Figure 1 reveals the WAXD scans of PPZn, m-PPZn and 5 wt% PBSA/m-PPZn nanocomposites. The WAXD data show that several strong diffraction peaks of PPZn and hexadecylamine-modified PPZn were obtained. The main diffraction peak of PPZn observed at 2θ = 6.31° agreed well with the previous literatures [12, 13]. The diffraction peaks of hexadecylamine-modified PPZn obtained at 2θ = 3.21° and 6.40°. These results demonstrate that the interlayer spacing determined using Bragg's equation was at 27.5 Å and 13.8 Å, respectively. The interlayer spacing of PPZn is extensively expanded with the addition of hexadecylamine through the interaction of ionic exchange. As the curve (c) presented in this figure, the diffraction peaks of PBSA/m-PPZn nanocomposites at 2θ = 19.4° (020), 21.5° (012), and 22.5° (110) suggested the crystal structure of PBSA/m-PPZn nanocomposites is the same compared to that of PBS [8, 14]. The diffraction peak of m-PPZn at 2θ = 3.21° was noticeably sharp and slightly shifted to the lower angle for the PBSA/m-PPZn nanocomposites. This implies that the PBSA polymer chain is intercalated into the m-PPZn galleries. This phenomenon probably results from disordered intercalated nanocomposite [15]. Therefore, the morphology of PBSA/m-PPZn

Preprints (www.preprints.org) | NOT PEER-REVIEWED | Posted: 21 May 2018 doi:10.20944/preprints201805.0269.v1

nanocomposites was examined by TEM analysis. Figure 2 reveals TEM micrographs of 5 wt% PBSA/m-PPZn nanocomposites. This data shows that the intercalated and agglomerated structures were observed.

In order to study the effect of m-PPZn on the structures of PBSA matrix, the SAXS analysis was performed. The Lorentz-corrected SAXS data of PBSA/m-PPZn nanocomposites isothermal crystallization at 66 °C are shown in Figure 3. To calculate the morphological factors, such as the amorphous thickness (l_a), the lamellar thickness (l_c), and long period ($L_p = l_a + l_c$), of all the materials, we used a one-dimensional correlation function. The one-dimensional correlation function, which is the Fourier transformation of Lorentz-corrected SAXS profiles, was evaluated as the following equation [16, 17]:

$$\gamma(z) = \frac{1}{Q}\int_0^\infty qI^2(q)\cos(qz)dq \quad (1)$$

where z is the correlation distance, Q is a scattering invariant, and $I(q)$ is the experimental SAXS intensity corrected for thermal fluctuations.

The morphological factors of the nanocomposites calculated from the one-dimensional correlation function are presented in Table 1. For the PBSA/m-PPZn nanocomposites, L_p and l_c values progressively decrease with the increasing hexadecylamine-modified PPZn contents. This result is probably contributed to the presence of hexadecylamine served as intercalation agents for PPZn, which might prevent the crystalline packing of PBSA crystallites. In addition, the l_a values slightly increase with the addition of m-PPZn. Therefore, the degree of crystallinity of the nanocomposites decreases compared to that of PBSA matrix.

Preprints (www.preprints.org) | NOT PEER-REVIEWED | Posted: 21 May 2018 doi:10.20944/preprints201805.0269.v1

Crystallization behavior

The isothermal crystallization kinetics of PBSA and PBSA/m-PPZn nanocomposites are determined by the following Avrami equation: [18, 19]

$$1 - X_t = \exp(-kt^n) \qquad (2)$$

where k and n are the Avrami parameters, depending on the nucleation and growth mechanisms of crystallites. The X_t is relative crystallinity at crystallization time t. In order to adapt easily with the operation, equation (2) can be rewritten into the following equation as Eq (3).

$$\ln[-\ln(1 - X_t)] = n \ln t + \ln k . \qquad (3)$$

The crystallization half-time ($t_{1/2}$) is defined as the time taken from the onset of the relative crystallinity until 50% completion, which is illustrated as equation (4).

$$t_{1/2} = \left(\frac{\ln 2}{k}\right)^{1/n} \qquad (4)$$

The plots of ln[-ln (1-X_t)] versus ln t for PBSA/m-PPZn nanocomposites are showed in Figure 4. All drawings show similar tendency, suggesting that the crystallization mechanism of PBSA/m-PPZn nanocomposites at various T_{cs} remains the same. The n values, k values, and $t_{1/2}$ at *various* T_{cs} are summarized in Table 2. The n value used in the Avrami expression represents the mechanism of crystal growth and nucleation. The n values of PBSA listed in Table 2 are found to range from 2.52 to 3.09. Generally, the n values near to 3 are assigned to an athermal nucleation process subsequently a three-dimensional crystal growth. The n values of PBSA/m-PPZn nanocomposites ranged from 2.75 to 3.38 are similar to those of PBSA. Thus, these data propose that the incorporation of m-PPZn into the

Preprints (www.preprints.org) | NOT PEER-REVIEWED | Posted: 21 May 2018 doi:10.20944/preprints201805.0269.v1

PBSA doesn't alter the mechanism of PBSA crystallization. Additionally, $t_{1/2}$ for the all samples shown in Table 2 increases as T_c increases, recommending that the isothermal crystallization rate decreases with increasing T_c, owing to the lower supercooling at higher T_c. With the additional loading of 3 wt% m-PPZn into PBSA, the $t_{1/2}$ significantly decreases as the content of m-PPZn increases. For example, the $t_{1/2}$ values of PBSA decrease remarkably from 8.80 to 5.88 min in nanocomposites with 3 wt % m-PPZn contents when crystallized at T_c = 70°C. This implies that m-PPZn could speed up the crystallization of PBSA in the nanocomposites. Nevertheless, by adding m-PPZn into PBSA up to 5 wt%, the $t_{1/2}$ of the PBSA/m-PPZn nanocomposite was remarkably increased. These data indicate that high loading of m-PPZn might reduce the free volume of the polymer and then delay the diffusion and migration of PBSA polymer chains to the crystalline packing and formation owing to the restriction effects, causing the increase of $t_{1/2}$.

The nucleation and crystalline morphologies of PBSA/m-PPZn nanocomposites were studied using polarized optical micrographs to supplementary expose the crystallization behaviors of the PBSA/m-PPZn nanocomposites. Figure 5 illustrates the growth of spherulites isothermally crystallized at 66 °C. The number of spherulites of the PBSA/m-PPZn nanocomposites at the same T_c clearly increases and the spherulite size decreases by adding 3 wt% m-PPZn. This result indicates that the incorporation of m-PPZn increased the amount of heterogeneous nucleation in the PBSA matrix. Nevertheless, the spherulite size of 5 wt% PBSA/m-PPZn nanocomposite turns out to be bigger, and the number of spherulites becomes less as the addition of 5wt% m-PPZn. This finding reveals that high

Preprints (www.preprints.org) | NOT PEER-REVIEWED | Posted: 21 May 2018 doi:10.20944/preprints201805.0269.v1

loading of m-PPZn could prevent the PBSA chain motion due to the possible interaction of m-PPZn and organic modifier, causing the reduction of nucleation.

The effects of m-PPZn on the PBSA spherulitic growth rate (G) shown in Table 2 were also determined using POM data. It is found that the G values decreased as T_c increases and the G values at a specified T_c decreased with the increase in the weight fraction of m-PPZn.

Biodegradability of PBSA/m -PPZn nanocomposites

The microbial biodegradability of PBSA/m-PPZn nanocomposites was shown in Figure 6. It can be seen that the weight loss of PBSA/m-PPZn nanocomposites increases as the degradation time increases. While the weight loss of the PBSA reached 51.5% after 96-h incubation, the weight loss of the 1 wt% PBSA/m-PPZn, 3 wt% PBSA/m-PPZn and 5 wt% PBSA/m-PPZn nanocomposites were 54.8, 62.4, and 71.9%, respectively. It can be seen that the degradation rates of all nanocomposites showed similar tendency compared to that of neat PBSA matrix. The degradation rate of the neat PBSA is slowest, but the degradation rate of the 5 wt% PBSA/m-PPZn nanocomposites is fastest compared to those of PBSA/m-PPZn nanocomposites.

To observe the change of morphologies for all the specimens subsequent to the degradation, the analysis technique of FESEM can be applied. The FESEM images of the surfaces before and after microbial degradation are presented in Figure 7. Before degradation, all samples show similar morphology and the surfaces of PBSA were pretty flat compared to those of the nanocomposites. The surface condition of PBSA/m-PPZn nanocomposites got more and more damaged within the incubation

 doi:10.20944/preprints201805.0269.v1

time course. After 2 days of incubation, the surface wearing away with the presence of small amount of porous structures on PBSA were obtained. After the same degradation time, the surface erosion of all nanocomposites contains more porous and holes structures. It can also be observed that the roughness of the PBSA nanocomposites surface as the loading of m-PPZn increases, demonstrating that the addition of the m-PPZn into PBSA polymer matrix drastically improves the degradation rate of PBSA.

It is recognized that internal structural factors and external environmental factors, such as chemical structure, degree of crystallinity, molecular weight, temperature, relative humidity, and pH value, have an effect on the degradation rate of biodegradable polymers [20]. This study of the microbial degradation was designed with the same external environment condition. Besides, the chemical structure for PBSA matrix is the same and initial molecular weight for PBSA matrix is almost identical. The only difference in this study is mainly contributed from the degree of crystallinity. In accordance with the WAXD data, the ranking of degree of crystallinity was PBSA > 1 wt% PBSA/m-PPZn nanocomposites > 3 wt% PBSA/m-PPZn nanocomposites > 5 wt% PBSA/m-PPZn nanocomposites. For 5 wt% PBSA/m-PPZn nanocomposites, the fastest degradation rate was achieved due to the lowest degree of crystallinity. Thus, the degradation rate altered in the ranking 5 wt% PBSA/m-PPZn nanocomposites > 3 wt% PBSA/m-PPZn nanocomposites > 1 wt% PBSA/m-PPZn nanocomposites > neat PBSA. It is also necessary to point out that the change of degree of crystallinity and degradation rate are almost linearly proportional to the loading of hexadecylamine-modified PPZn, which is totally different from other organically-modified PPZn/PBSA systems [21]. This finding

 doi:10.20944/preprints201805.0269.v1

would provide an important information for the manufacturing biodegradable PBSA nanocomposites.

Two categories, such as the exo- and endo-type hydrolysis activity, were used to explain the degradation behavior of biodegradable polymers. They considerably depend on the change of weight-average molecular weight (M_w) of the biodegradable polymers [22]. The exo-type hydrolysis activity is followed if the M_w doesn't vary extensively during the degradation process. This degradation behavior reveals that the degradation initiates from both sides of the PBSA polymer chains [22]. In contrast, the endo-type hydrolysis activity is obeyed if M_w significantly decreases during the degradation process. This occurrence is ascribed to the degradation begins at the midpoint of the PBSA polymer chain. The M_w change of PBSA/m-PPZn nanocomposites after microbial degradation is shown in Figure 8. The polymer dispersity index (PDI) of all samples is recorded in Table 3. This result indicates that the change of M_w of PBSA is very little as the weight loss of PBSA steadily increases. Therefore, the degradation behavior of the PBSA is contributed to the exo-type hydrolysis activity, which is in good agreement with the previous studies [22, 23]. Nevertheless, the degradation performance of PBSA/m-PPZn nanocomposites is extremely analogous to those of PBSA. These data point out that the addition of the m-PPZn into PBSA doesn't alter the degradation performance of PBSA.

CONCLUSIONS

The biocompatible and biodegradable PBSA/hexadecylamine-modified PPZn nanocomposites were manufactured using a melt mixing process. The results of WAXD and TEM revealed that the

 doi:10.20944/preprints201805.0269.v1

structure of PBSA/m-PPZn nanocomposites contained the mixture of exfoliated and intercalated form. Degradation tests results show that the weight loss of PBSA increases as the loading of m-PPZn increases. This result is attributed to the lower degree of crystallinity for the PBSA/m-PPZn nanocomposites. The degradation performance of PBSA determined using the change of weight-average molecular weight is contributed to the exo-type hydrolysis activity as a result of the degradation initiates from both sides of the PBSA polymer chains.

ACKNOWLEDGEMENTS

The work was supported by the Ministry of Science and Technology (MOST) under Grand MOST 104-2212-E-005-089-MY2 and the Minister of Education under the project of Innovation and Development Center of Sustainable Agriculture (IDCSA).

 doi:10.20944/preprints201805.0269.v1

REFERENCES

1. Ojijo, V.; Ray, S. S. Nano-biocomposites based on synthetic aliphatic polyesters and nanoclay. *Prog. Mater. Sci.,* **2014**, *62*, 1–57.

2. Chen, Y. A.; Hang, Y. T.; Wu, T. M. Polymorphism and spherulite morphology of poly (1,4-butylene adipate)/organically-modified layered double hydroxide nanocomposites. *J. Appl. Polym. Sci*., **2015**, *132*, 42526.

3. Ray, S. S.; Bousmina, M.; Okamoto, K. Structure and properties of nanocomposites based on poly (butylene succinate-co-adipate) and organically modified montmorillonite. *Macro. Mater. Eng.*, **2005**, *290*, 759-768.

4. Qi, Z.; Ye, H.; Xu, J.; Chen, J.; Guo, B. Improved the thermal and mechanical properties of poly(butylene succinate-co-butylene adipate) by forming nanocomposites with attapulgite. *Colloids Surf. A Physicochem. Eng. Asp*., **2013**, *421*, 109-117.

5. Bandyopadhyay, J., Al-Thabaiti, S. A.; Ray, S. S.; Basahel, S. N.; Mokhtar, M. Unique cold-crystallization behavior and kinetics of biodegradable poly[(butylene succinate)-co adipate] nanocomposites: a high speed differential scanning calorimetry study. *Macromol. Mater. Eng*., **2014**, *299*, 939-952.

6. Ojijo, V.; Malwela, T.; Ray, S. S.; Sadiku, R. Unique isothermal crystallization phenomenon in the ternary blends of biopolymers polylactide and poly[(butylene succinate)-co-adipate] and nano-clay. *Polymer*, **2012**, *53*, 505-518.

7. Ojijo, V.; Ray, S. S.; Sadiku, R. Effect of nanoclay loading on the thermal and mechanical properties of biodegradable polylactide/poly[(butylene succinate)-co-adipate] blend composites. *ACS Appl. Mater. Interfaces*, **2012**, *4*, 2395-2405.

8. Chen, Y. A.; Tsai, G. S.; Chen, E. C.; Wu, T. M. Crystallization behaviors and microstructures of poly(butylene succinate-co-adipate)/modified layered double hydrox ide nanocomposites. *J. Mater. Sci*., **2016**, *51*, 4021-4030.

9. Pan, P.; Liang, Z.; Cao, A.; Inoue, Y. Layered metal phosphonate reinforced poly(l-lactide) composites with a highly enhanced crystallization rate. *ACS Appl. Mat. Interfaces,* **2009**, *1*, 402-411.

10. Xu, T.; Wang, Y.; He, D.; Xu, Y.; Li, Q.; Shen, C. Nucleation effect of layered metal phosphonate on crystallization of isotactic polypropylene. *Polym. Test,* **2014**, *34*, 131-139.

11. Wu, N.; Wang, H. Effect of zinc phenylphosphonate on the crystallization behavior of poly (l-lactide). *J. Appl. Polym. Sci*., **2013**, *130*, 2744-2752.

12. Chen, Y. A.; Chen, E. C.; Wu, T. M. Lamellae evolution of stereocomplex-type poly(lactic acid)/organically-modified layered zinc phenylphosphonate nanocomposites induced by isothermal crystallization. *Materials*, **2016**, *9*, 159.

13. Chen, Y. A.; Chen, E. C.; Wu, T. M. Organically modified layered zinc phenylphosphonate reinforced stereocomplex-type poly (lactic acid) nanocomposites with highly enhanced mechanical properties and degradability. *J. Mater. Sci*., **2015**, *50*, 7770-7778.

 doi:10.20944/preprints201805.0269.v1

14. Chen, Y. A.; Tsai, G. S.; Chen, E. C.; Wu, T. M. Thermal degradation behaviors and biodegradability of novel nanocomposites based on various poly[(butylene succinate)-co-adipate] and modified layered double hydroxides. *J. Taiwan Inst. Chem. Eng*., **2017**, *77*, 263-270.

15. Gilman, J. W.; Morgan, A. B. Characterization of polymer-layered silicate (clay) nanocomposites by transmission electron microscopy and X-ray diffraction: A comparative study. *J. Appl. Polym. Sci.*, **2003**, *87*, 1329-1338.

16. Strobl, G.; Schneider, M. Direct evaluation of the electron density correlation function of partially crystalline polymers. *J. Polym. Sci. Polym. Phys. Ed*., **1980**, *18*, 1343-1359.

17. Barbi, V.; Funari, S. S.; Gehrke, R.; Scharnagl, N.; Stribeck, N. SAXS and the Gas Transport in Polyether-block-polyamide Copolymer Membranes. *Macromolecules*, **2003**, *36*, 749-758.

18. Avrami, M. Granulation, Phase Change, and Microstructure Kinetics of Phase Change. III. *J. Chem. Phys*., **1941**, *9*, 177-184.

19. Avrami, M. Kinetics of Phase Change. II Transformation-Time Relations for Random Distribution of Nuclei. *J. Chem. Phys*., **1940**, *8*: 212-224.

20. Numata, K.; Finne-Wistrand, A.; Albertsson, A. C.; Doi, Y.; Abe, H. Enzymatic degradation of monolayer for poly(lactide) revealed by real-time atomic force microscopy: effects of stereochemical structure, molecular weight, and molecular branches on hydrolysis rates. *Biomacromolecules*, **2008**, *9*: 2180-2185.

21. Chen, Y. A.; Kuo, D. L.; Chen, E. C.; Wu, T. M. Enhanced enzymatic degradation in

 doi:10.20944/preprints201805.0269.v1

nanocomposites of various organically-modified layered zinc phenylphosphonates and poly (butylene succinate-co-adipate). *J. Polym. Res.*, **2017**, *24*, 212.

22. Ando, Y.; Yoshikawa, K.; Yoshikawa, T.; Nishioka, M.; Ishioka, R.; Yakabe, Y. Biodegradability of poly(tetramethylene succinate-co-tetramethylene adipate): I. Enzymatic hydrolysis. *Polym. Degrad. Stab*., **1998**, *61*, 129-137.

23. Ciou, C. Y.; Li, S. Y.; Wu, T. M. Morphology and degradation behavior of poly (3-hydroxybutyrate-co-3-hydroxyvalerate)/layered double hydroxides composites. *Eur. Polym. J*., **2014**, *59*, 136-143.

Preprints (www.preprints.org) | NOT PEER-REVIEWED | Posted: 21 May 2018 doi:10.20944/preprints201805.0269.v1

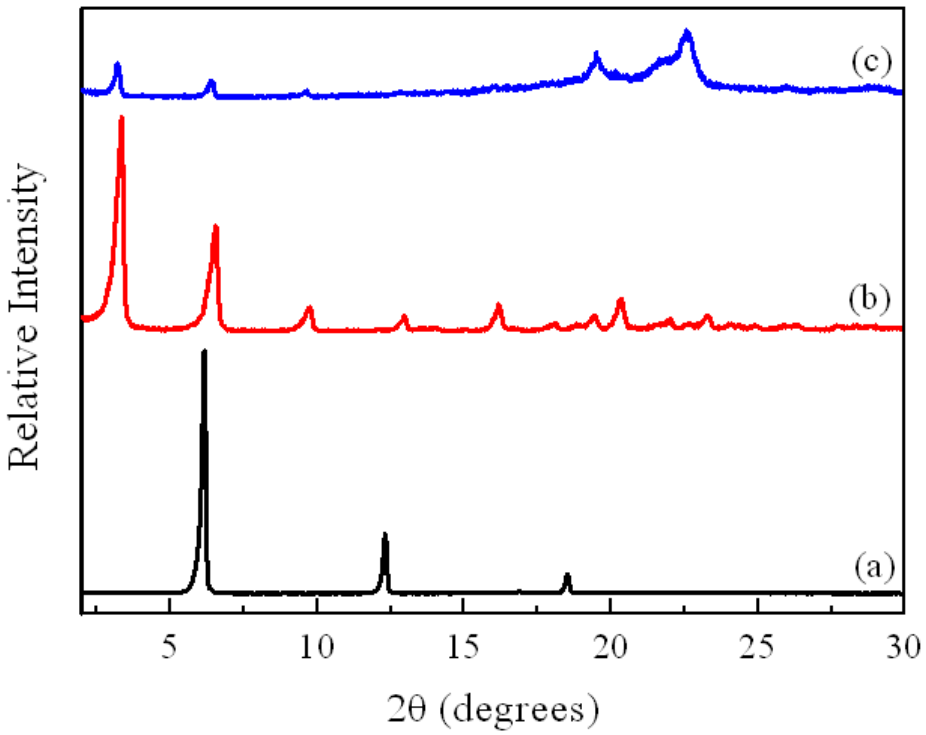

Figure 1: X-ray diffraction patterns of (a) PPZn, (b) m-PPZn and (c) 5 wt% PBSA/m-PPZn nanocomposite.

Preprints (www.preprints.org) | NOT PEER-REVIEWED | Posted: 21 May 2018 doi:10.20944/preprints201805.0269.v1

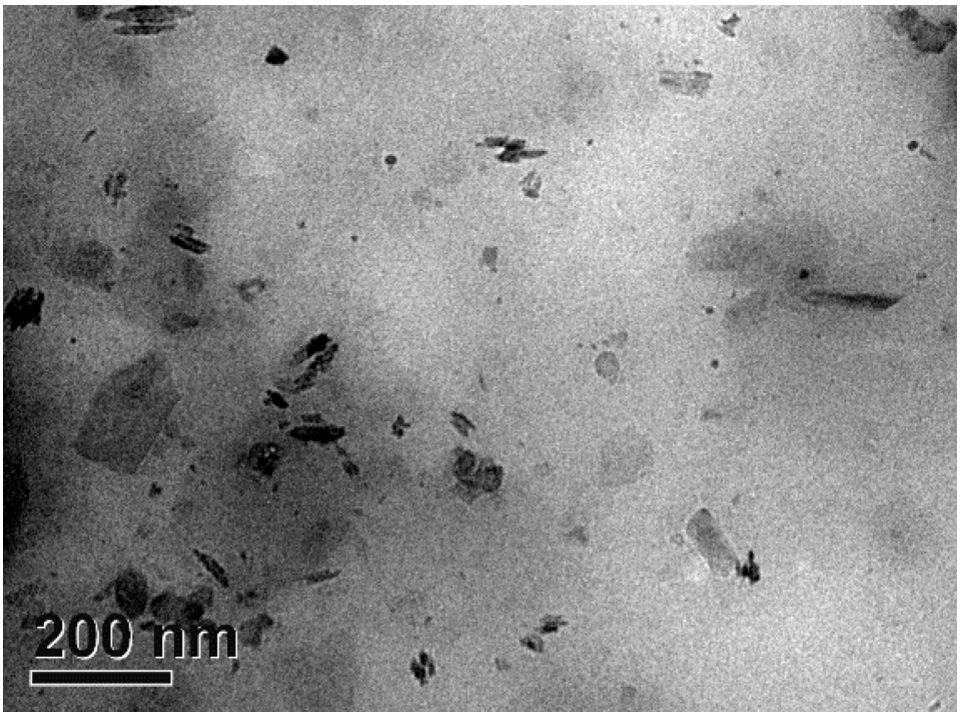

Figure 2: TEM micrographs of 5 wt% PBSA/m-PPZn nanocomposites.

Preprints (www.preprints.org) | NOT PEER-REVIEWED | Posted: 21 May 2018 doi:10.20944/preprints201805.0269.v1

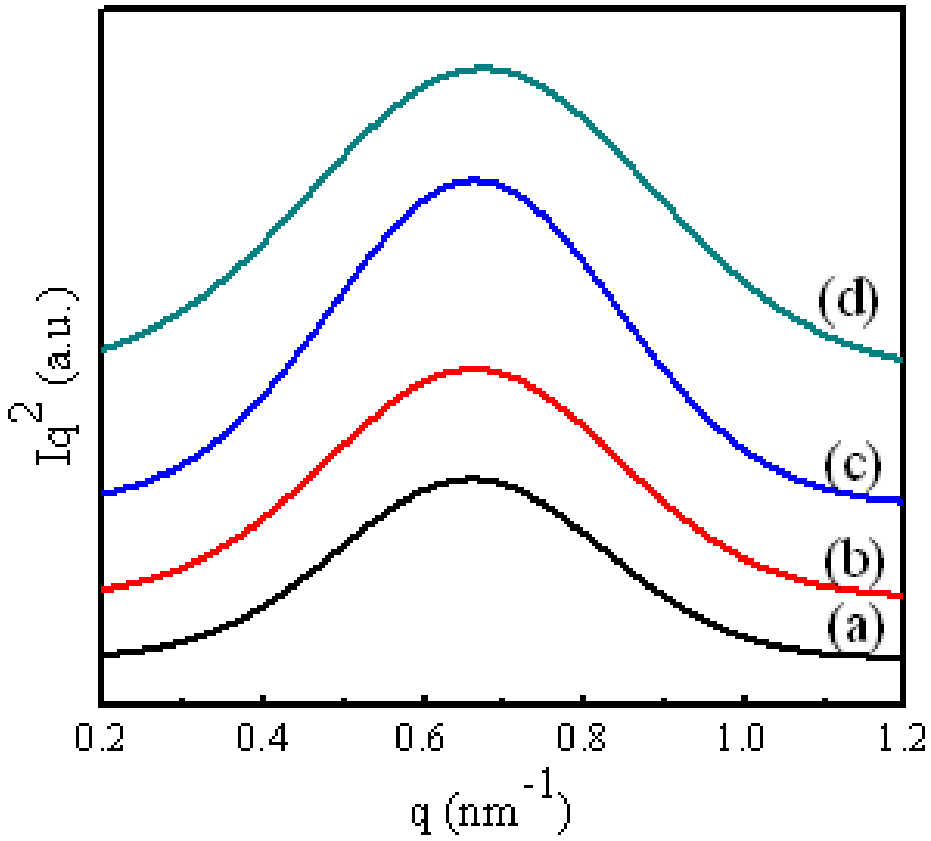

Figure 3: Lorentz-corrected SAXS intensity profiles of (a) neat PBSA, (b) 1 wt% PBSA/m-PPZn, (c) 3 wt% PBSA/m-PPZn, and (d) 5 wt% PBSA/m-PPZn nanocomposites during isothermal crystallization at 66 °C.

Preprints (www.preprints.org) | NOT PEER-REVIEWED | Posted: 21 May 2018 doi:10.20944/preprints201805.0269.v1

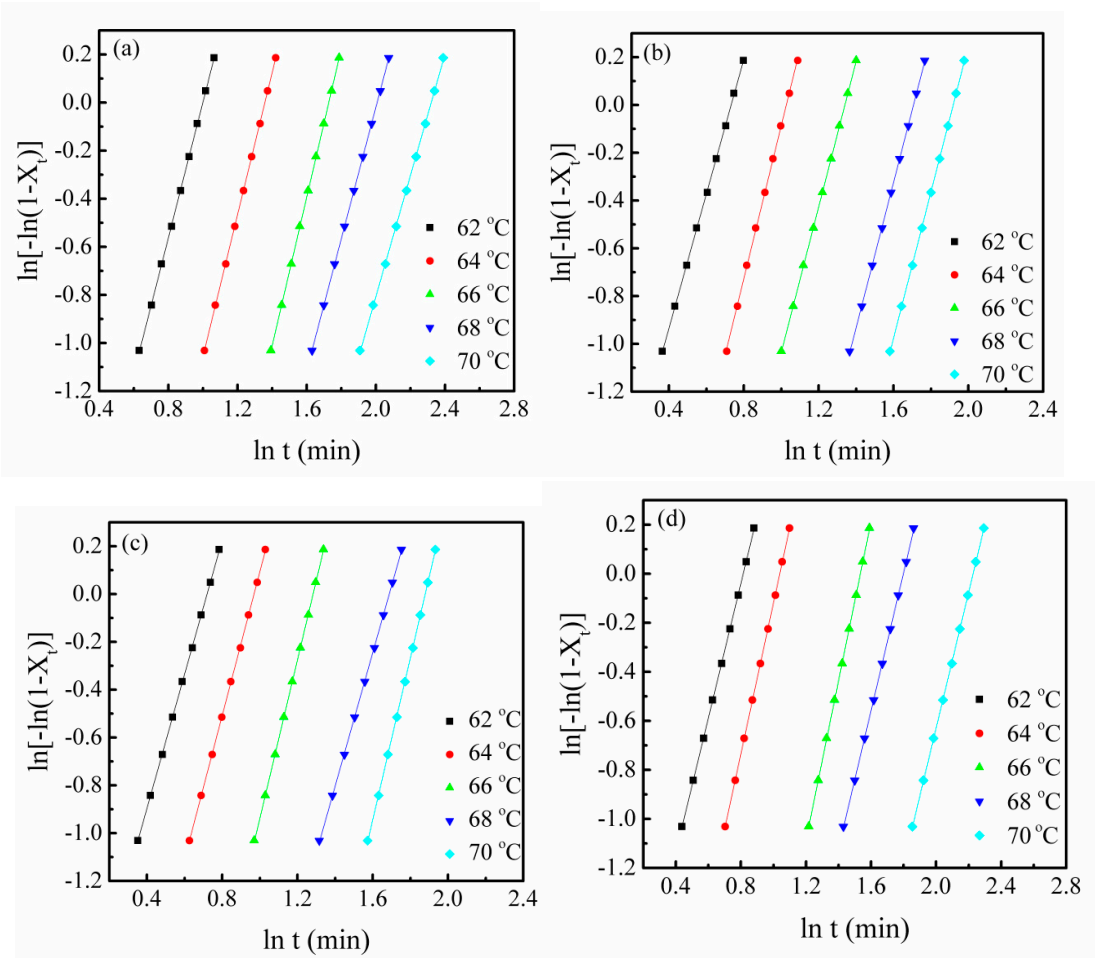

Figure 4: Avrami plots of (a) neat PBSA, (b) 1 wt% PBSA/m-PPZn, (c) 3 wt% PBSA/m-PPZn, and (d) 5 wt% PBSA/m-PPZn nanocomposites isothermal crystallization at various temperatures.

Preprints (www.preprints.org) | NOT PEER-REVIEWED | Posted: 21 May 2018 doi:10.20944/preprints201805.0269.v1

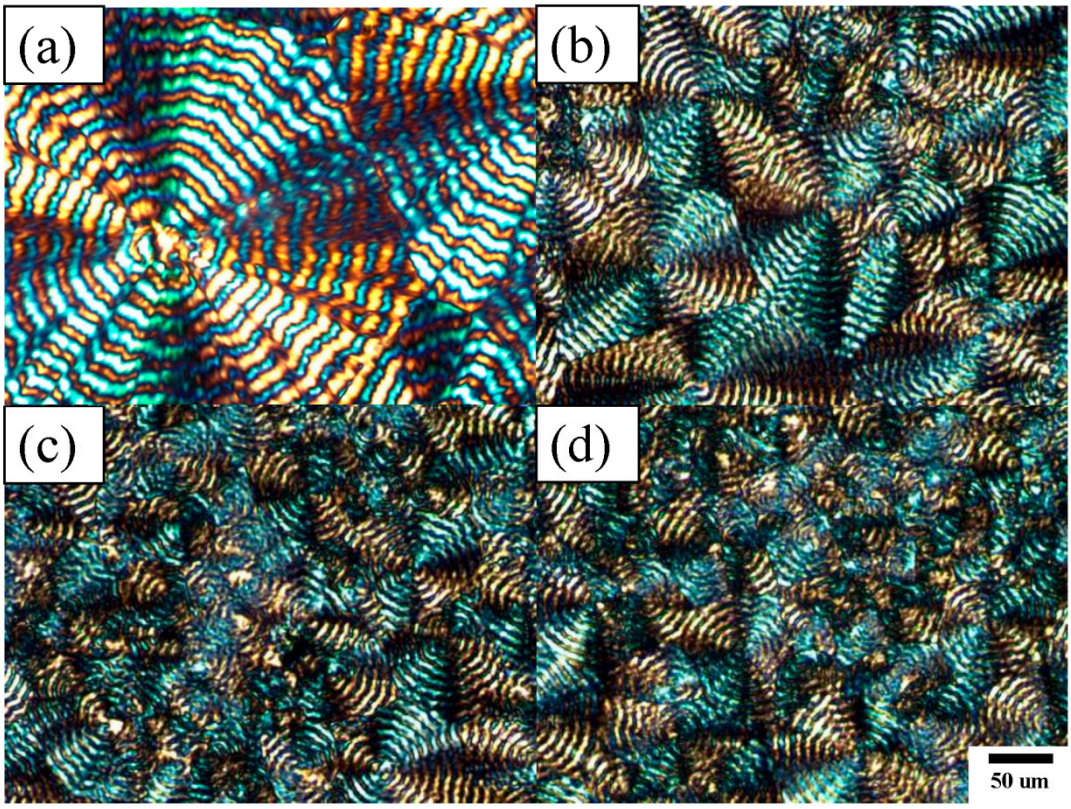

Figure 5: Optical micrographs of spherulites of (a) neat PBSA, (b) 1 wt% PBSA/m-PPZn, (c) 3 wt% PBSA/m-PPZn, and (d) 5 wt% PBSA/m-PPZn nanocomposites during isothermal crystallization at 66 °C.

Preprints (www.preprints.org) | NOT PEER-REVIEWED | Posted: 21 May 2018 doi:10.20944/preprints201805.0269.v1

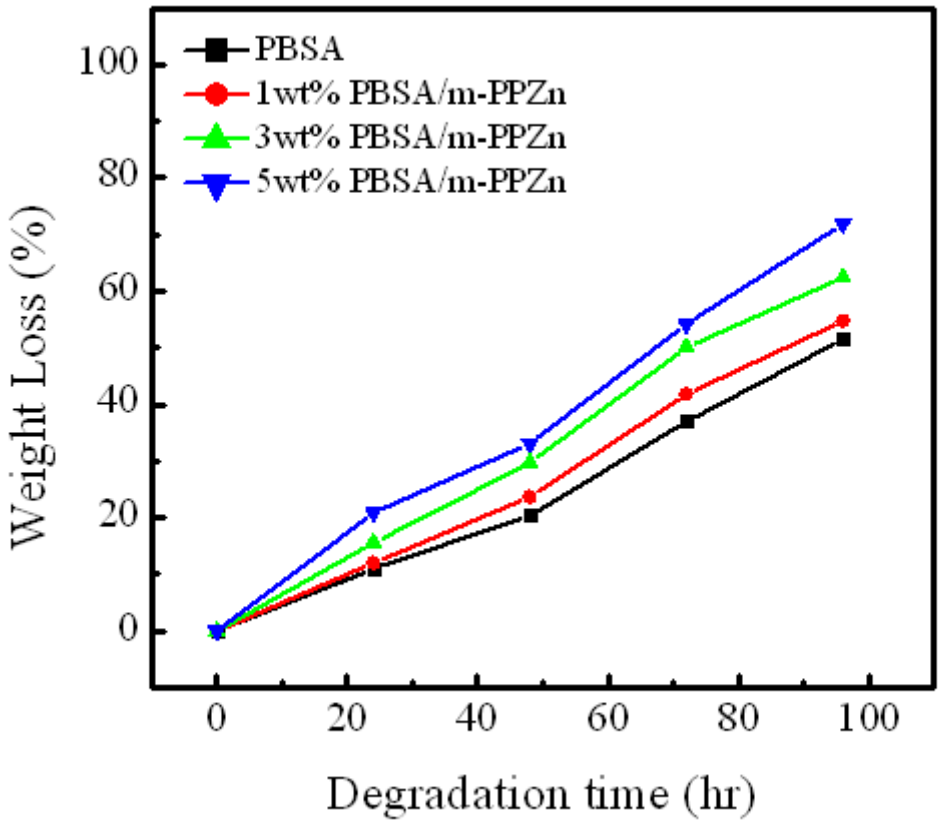

Figure 6: Dependence of the weight loss on the degradation time of PBSA/m-PPZn nanocomposites.

Preprints (www.preprints.org) | NOT PEER-REVIEWED | Posted: 21 May 2018 doi:10.20944/preprints201805.0269.v1

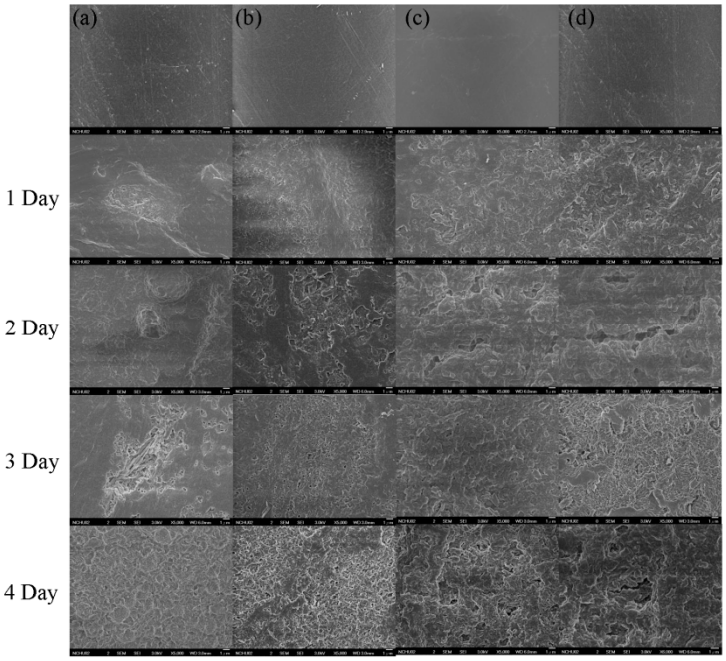

Figure 7: FESEM images of the microbially degraded (a) neat PBSA, (b) 1 wt% PBSA/m-PPZn, (c) 3 wt% PBSA/m-PPZn, and (d) 5 wt% PBSA/m-PPZn nanocomposites.

Preprints (www.preprints.org) | NOT PEER-REVIEWED | Posted: 21 May 2018 doi:10.20944/preprints201805.0269.v1

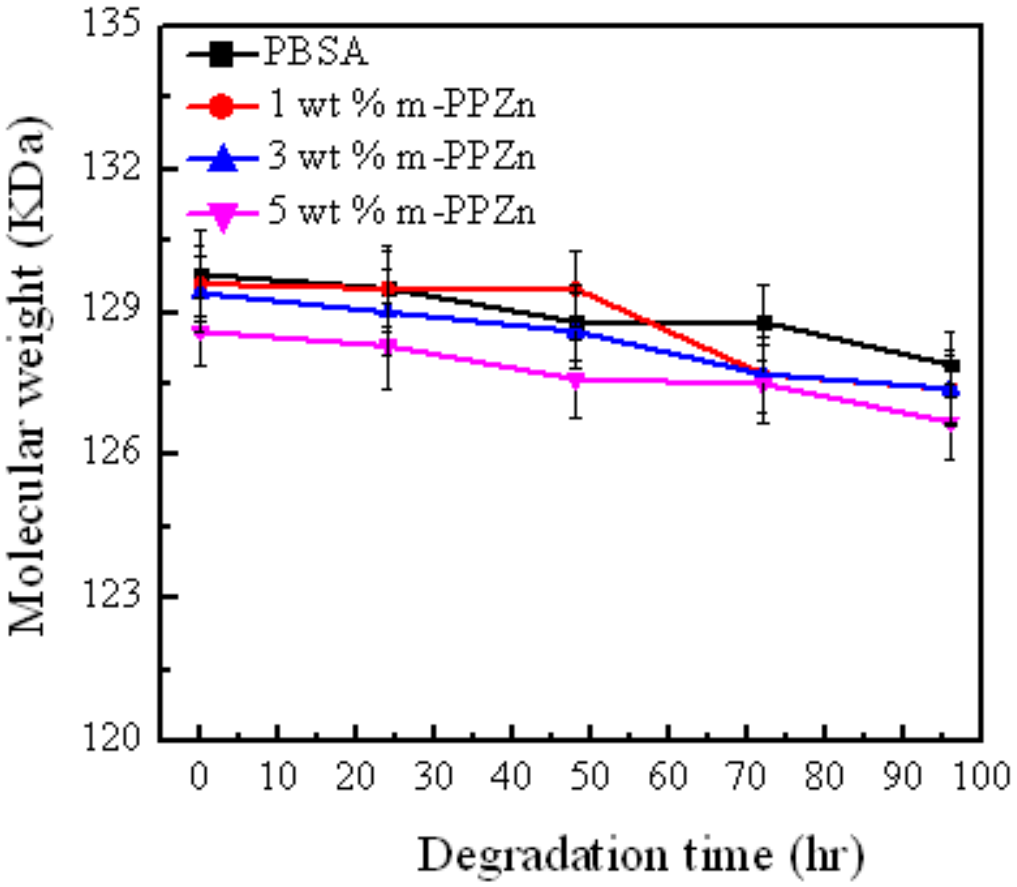

Figure 8: Molecular weight of residual PBSA/m-PPZn nanocomposites after the microbial degradation.

Preprints (www.preprints.org) | NOT PEER-REVIEWED | Posted: 21 May 2018 doi:10.20944/preprints201805.0269.v1

Table 1. Structural parameters of PBSA and PBSA/m-PPZn nanocomposites crystallized at T_c of 66 ºC estimated by XRD and SAXS measurements.

Sample	Temp. (ºC)	Xc (%)	L_P (nm)	l_c (nm)	l_a (nm)
PBSA	66	47.09	8.24	3.40	4.84
1 wt % PBSA/m-PPZn	66	46.42	8.23	3.33	4.90
3 wt % PBSA/m-PPZn	66	42.83	8.19	3.23	4.96
5 wt % PBSA/m-PPZn	66	40.14	7.99	3.11	4.88

Preprints (www.preprints.org) | NOT PEER-REVIEWED | Posted: 21 May 2018 doi:10.20944/preprints201805.0269.v1

Table 2. Kinetic parameters of neat PBSA and PBSA/m-PPZn nanocomposites isothermally melt crystallized at T_c =62–70 °C.

Sample	T_c(°C)	n	k(min^{-n})	$t_{1/2}$(min)	G(μm/sec)
PBSA	62	2.82	5.9×10^{-2}	2.39	1.429
	64	2.95	1.82×10^{-2}	3.43	1.304
	66	3.09	4.81×10^{-3}	5.00	1.083
	68	2.74	4.10×10^{-3}	6.51	0.901
	70	2.52	2.88×10^{-3}	8.80	0.700
1wt % PBSA/m-PPZn	62	2.81	1.28×10^{-1}	1.83	1.160
	64	3.20	3.74×10^{-2}	2.49	0.988
	66	3.04	1.69×10^{-2}	3.39	0.821
	68	3.03	5.58×10^{-3}	4.89	0.618
	70	3.06	2.82×10^{-3}	6.05	0.444
3wt % PBSA/m-PPZn	62	2.81	1.33×10^{-1}	1.80	1.055
	64	3.01	5.43×10^{-2}	2.33	0.851
	66	3.32	1.42×10^{-2}	3.23	0.665
	68	2.79	8.97×10^{-3}	4.74	0.520
	70	3.38	1.73×10^{-3}	5.88	0.347
5wt % PBSA/m-PPZn	62	2.75	1.07×10^{-1}	1.98	0.930
	64	3.07	4.11×10^{-2}	2.51	0.768
	66	3.25	6.83×10^{-3}	4.15	0.583
	68	2.81	6.35×10^{-3}	5.30	0.442
	70	2.77	2.10×10^{-3}	8.13	0.268

Preprints (www.preprints.org) | NOT PEER-REVIEWED | Posted: 21 May 2018 doi:10.20944/preprints201805.0269.v1

Table 3. PDI of PBSA/m-PPZn obtained by GPC measurements with various degradation times.

Sample	PDI				
	0hr	24hr	48hr	72hr	96hr
PBSA	1.47	1.50	1.51	1.53	1.59
1 wt % PBSA/m-PPZn	1.47	1.48	1.53	1.52	1.57
3 wt % PBSA/m-PPZn	1.48	1.50	1.54	1.54	1.61
5 wt % PBSA/m-PPZn	1.49	1.54	1.55	1.59	1.64